1992ApJ...389..546B

THE ASTROPHYSICAL JOURNAL, 389:546–557, 1992 April 20
© 1992. The American Astronomical Society. All rights reserved. Printed in U.S.A.

THREE-DIMENSIONAL HYDRODYNAMICAL SIMULATIONS OF COLLIDING STARS. III. COLLISIONS AND TIDAL CAPTURES OF UNEQUAL-MASS MAIN-SEQUENCE STARS

W. BENZ[1]
Harvard-Smithsonian Center for Astrophysics, 60 Garden Street, Cambridge, MA 02138
AND
J. G. HILLS
Theoretical Division, T-6, MS B288, Los Alamos National Laboratory, Los Alamos, NM 87545
Received 1991 August 5; accepted 1991 October 24

ABSTRACT

We used a three-dimensional smooth-particle hydrodynamics (SPH) code with 7000 particles to simulate 30 collisions between lower main-sequence (MS) stars whose masses differ by a factor of 5. We also simulated encounters with point-mass intruders to understand better how the finite radius of the intruder affects the dynamics. The two MS stars become gravitationally bound in a physical collision if their relative velocity, V, at infinity is less than a critical (dissipation) velocity, V_d. We find that V_d decreases from 1000 km s^{-1} in a head-on collision to 150 km s^{-1} in a grazing one. If the less massive star is replaced by a point mass (e.g., a white dwarf), V_d remains the same for grazing collisions and tidal encounters, but it drops to $\sim$600 km s^{-1} in head-on collisions. If $V > V_d$, the lower mass ms star, which is the denser of the two, passes through the more massive MS star and escapes without becoming gravitationally bound to it. In collisions between two main-sequence stars, V_d increases with V due to increased shock dissipation. In collisions between a point mass and a main-sequence star, V_d decreases as V increases. The only dissipation in these cases is by gravitationally induced oscillations that decrease in importance as V increases. If the two MS stars coalesce in a physical collision, the denser (lower mass) MS star settles to the center of the other one. The violent mixing of the more massive star during the encounter and the settling of the low-mass star to its center should reset the nuclear clock of the coalesced star, so it contracts to the (helium-rich) MS. The fraction of the stellar mass lost in these collisions is much less than that lost in collisions between stars of equal mass and density. In particular, grazing collisions do not produce the large mass loss and accretion disks that characterize collisions between equal-mass stars. We find that tidal captures of binary stars in globular clusters can only occur in encounters in which the closest approach of the two stars to their center of mass is less than 2.0 times the sum of their radii. Coalescence of two MS stars in a globular cluster is more probable than their forming a binary by tidal capture. Tidal capture is not possible if the impact velocity at infinity exceeds 150 km s^{-1}. Even at zero impact velocity, the coalesced star acquires a kick velocity of up to 4.5 km s^{-1} by asymmetric jetting during the collision. This velocity is not enough to eject the coalesced star from a globular cluster, but it largely compensates for the dynamical cooling resulting from the coalescence of the two stars. The coalescence of stars in globular clusters does not speed up the dynamical collapse of the core of the cluster.

Subject headings: celestial mechanics, stellar dynamics — globular clusters: general — hydrodynamics — methods: numerical

1. INTRODUCTION

Collisions between main-sequence (MS) stars are important in the cores of globular clusters (Hills & Day 1976) and in galactic nuclei. In the two earlier papers in this series we have the results of collisions between equal-mass MS stars (Benz & Hills 1987, hereafter Paper I) and between white dwarfs (Benz, Hills, & Thielemann 1989, hereafter Paper II). These papers list references to earlier work on stellar collisions and to the basic characteristics of the SPH code used in these simulations. Collisions with giant stars have been studied by Davies, Benz, & Hills (1991).

In this paper, we investigate collisions and close encounters between unequal-mass MS stars. We also simulate collisions between point-mass intruders (white dwarfs) and MS stars to understand better how the physics of the encounters depends on the finite radius of the smaller MS star.

The masses of the two stars differ by a factor of 5, which should represent cases in which the two stars differ significantly in mass. We treat each preencounter star as a polytrope of index $n = 1.5$, which is a good approximation for the lower MS stars that dominate both globular clusters and galactic nuclei where most physical collisions occur.

The fusion of hydrogen to helium in the cores of MS stars supports their luminosity. Because the rate of energy production by this mechanism increases rapidly with increasing temperature, the mean temperature in the cores of MS stars increases slowly with increasing MS mass despite the huge increase in MS luminosity. If there were no increase in temperature, the virial theorem would require the radius of a MS star to be proportional to its mass. In our simulations, with the more massive star having a mass and radius of unity, the less massive star has a mass and radius of 0.2 and 0.2532, respectively. If the more massive star has a solar mass and radius, the other star has the radius of a MS star with a mass of 0.2 $M_\odot$. The lower mass MS star is 12.3 times more dense than the more massive one.

[1] Now at Steward Observatory, University of Arizona, Tucson, AZ 85721.

© American Astronomical Society • Provided by the NASA Astrophysics Data System

1992ApJ...389..546B

Our collisions between MS stars differ significantly from the collisions of the "stars" given in Cleary & Monaghan (1990), who give the polytropes the same specific entropy, which results in the more massive object being denser, which is exactly opposite to the mass-density behavior of MS stars.

In § 2 we describe the assumptions and numerical techniques used in our calculations. In § 3 we describe the initial conditions, and in § 4 we give the results.

2. ASSUMPTIONS AND NUMERICAL TECHNIQUES

Our calculations ignore radiation transport, which is a reasonable simplification. All shocks except those in the outer atmosphere (which the code does not model) occur in optically thick regions where heat transport is on a diffusion time scale, which much exceeds the shock crossing time. We also ignore complications such as magnetic fields and consider the two colliding stars as an isolated system.

As in our previous paper on equal-mass MS star collisions (Paper I), we neglect nuclear energy release because the time during which the temperature exceeds hydrogen ignition threshold is too short for any significant generation of energy.

The evolution of the system is described by the three-dimensional hydrodynamics conservation equations. To solve this system of equations we use, as in Paper I and II, the Smoothed Particle Hydrodynamics (SPH) method. This method has been described extensively in the literature (for example, Benz 1990) as have a number of tests to check its ability to reproduce analytical and experimental results (see, for example, Monaghan 1985; Benz 1988, and references therein). Here, we shall only point out the slight modifications made to the now "standard" versions of SPH.

The finite extent of the Lagrangian particles is determined by a smoothing function (or kernel) containing a characteristic length scale h. This length scale is roughly analogous to a zoning scale in conventional finite difference methods. In this paper we use the kernel called W_4 in Monaghan & Lattanzio (1985) which is based on B-splines rather than the exponential kernel used in Paper I. The smoothing length h was allowed to change both in time and space according to the following evolution equation solved in parallel to the hydrodynamics equations (Benz 1990):

$$\frac{dh}{dt} = \frac{1}{3} h \nabla \cdot \boldsymbol{v} . \tag{2.1}$$

This provides a smooth variation of h consistent with the SPH technique and ensures that the number of interacting neighbors with any given particle remains roughly constant.

The time integration in our code is done using a second-order Runge-Kutta-Fehlberg integrator. As discussed by Benz (1990), this method, although requiring two force evaluations per time step, is at least as fast as the commonly used leap-frog scheme (Hernquist & Katz 1989) with time steps limited by the Courant-Friedrichs-Lewy condition. It has the additional advantage to be simpler since all quantities (velocities, positions, etc.) are defined at the same time. This is especially important when additional evolution equations (magnetic field, etc.) have to be solved simultaneously to second order as well. Furthermore, each particle is integrated with its own time step determined from the requirement that the truncation error estimate remains less than a preset tolerance.

Local conservation of linear momentum is achieved by proper symmetrization of the forces. In our code, we symmetrize the smoothing length, $h_{ij} = (h_i + h_j)/2$, rather than the kernel (Hernquist & Katz 1989) to compute particle-particle interactions.

Finally, we use the hierarchical binary tree to determine the gravitational potential and force that has been described in Benz et al. (1990).

3. INITIAL CONDITIONS

The two stars are modeled as polytropes of index $n = 1.5$, which approximates lower MS stars. There are initially 3500 fluid particles in each star. We treat the dynamics analytically as a two-body problem until the separation of the two stars is three times the sum of their radii where fully hydrodynamic calculations begin.

If the separation of the two stars is the sum of their radii and the more massive one has a solar mass and radius, then the escape velocity is

$$V_{\rm esc} = \left[\frac{2G(M_1 + M_2)}{(R_1 + R_2)}\right]^{1/2} = 604 \text{ km s}^{-1} . \tag{3.1}$$

We made simulations at many impact parameters for collision velocities at infinity, V, such that $V/V_{\rm esc} = 0$, 0.496, and 0.993, and 1.489, which correspond to $V = 0$, 300, 600, and 900 km s^{-1}, if the more massive star has a solar mass and radius. We have run collisions at zero impact parameters out to $V/V_{\rm esc} = 4.96$ or $V = 3000$ km s^{-1}.

Paper I showed that the results of a collision between two stars are nearly independent of V if $V \ll V_{\rm esc}$. $V_{\rm esc} \approx 600$ km s^{-1} for MS stars, so the results for 0 km s^{-1} should model collisions in globular clusters, in which colliding stars have $V = 10$–15 km s^{-1}. The velocity dispersion in galactic nuclei, including the Galactic Center, is typically 150–300 km s^{-1}, so the two lowest values of V used in our simulations should bracket the collisional velocities expected in galactic nuclei. The "collapse" of a galactic nucleus, in analogy to a globular cluster core "collapse," can raise the collision velocities significantly above 300 km s^{-1}. High-velocity collisions also occur near black holes in AGNs (Hills 1978). Our high-velocity collisions simulate the collisions expected in evolved galactic nuclei.

4. RESULTS

We describe the results of the individual collisions in this section. Table 1 gives the principal quantitative results.

Column (1) of Table 1 gives V, the impact velocity at infinity, in km s^{-1} as scaled to the particular case in which M_1 and R_1 have solar values. Column (2) gives $R_{\rm min}$, the projected minimum separation (periastron distance) of the two stars in the encounter if they were point masses. $R_{\rm min}$ is given in units of the sum of the stellar radii, $R_1 + R_2$. We calculate $R_{\rm min}$ analytically from the preencounter orbital angular momentum and kinetic energy. $R_{\rm min}$ is related to the impact parameter p and the impact velocity at infinity, V, by the equation

$$R_{\rm min} = a_c \left\{\left[1 + \left(\frac{p}{a_c}\right)^2\right]^{1/2} - 1\right\}, \tag{4.1}$$

or

$$\frac{p^2}{R_{\rm min}^2} = \left(1 + \frac{2a_c}{R_{\rm min}}\right) = \left[1 + \left(\frac{R_1 + R_2}{R_{\rm min}}\right)\left(\frac{V_{\rm esc}}{V}\right)^2\right], \tag{4.2}$$

© American Astronomical Society • Provided by the NASA Astrophysics Data System

1992ApJ...389..546B

TABLE 1

MAIN-SEQUENCE VERSUS MAIN-SEQUENCE ENCOUNTERS: MASSES 5/1

V (km s^{-1}) (1)	R_{min} ($R_1 + R_2$) (2)	ΔM_{12} ($M_1 + M_2$) (3)	ΔM_1 (ΔM_{12}) (4)	N (5)	V_f (km s^{-1}) (6)	V_d (km s^{-1}) (7)
0	0.000	0.0082	0.898	1	...	...
0	0.159	0.0124	0.935	1	...	...
0	0.250	0.0178	0.888	1	...	...
0	0.399	0.0256	0.871	1	...	...
0	0.500	0.0214	0.864	1	−465.0	465.0
0	0.638	0.0167	0.808	1	−338.9	338.9
0	0.757	0.0206	0.796	1	−240.6	240.6
0	1.00	0	0	1[a]	−153.1	153.1
0	1.2	0	0	1[a]	−99.3	99.3
0	1.4	0	0	1[a]	−58.8	58.8
0	1.6	0	0	1[a]	−30.6	30.6
0	1.8	0	0	1[a]	−9.4	9.4
300	0.0	0.0078	0.836	1	...	...
300	0.25	0.0238	0.912	1	...	...
300	0.399	0.0290	0.921	1	−540.9	618.5
300	0.65	0.0048	0.788	1[a]	−55.0	305
300	0.75	0.0020	0.840	2	197.4	225.9
600	0.0	0.0201	0.806	1	...	...
600	0.25	0.0561	0.909	1	−448.0	748.8
600	0.40	0.0261	0.904	2	59.7	597.0
600	0.50	0.0182	0.852	2	331.2	500.3
900	0.0	0.0903	0.946	1[a]	−258.3	936.3
900	0.10	0.0751	0.948	1[a]	−134.1	909.9
900	0.125	0.0712	0.954	2	265.4	860.0
900	0.2	0.0772	0.894	2	336.9	834.6
900	0.53	0.0278	0.853	2	681.5	587.8
975	0.0	0.0975	0.951	1[a]	−65.3	977
1200	0.0	0.1496	0.969	2	463.3	1107
1971	0.0	0.4444	0.955	2	1165.3	1590
3000	0.0	1.0	0.833	0	...	...

[a] Encounter not followed to final coalescence.

where

$$a_c = \frac{G(M_1 + M_2)}{V^2}, \tag{4.3}$$

is the "accretion" radius that parameterizes gravitational focusing. Here V_{esc} is the escape velocity given by equation (3.1) if $R_{min} = (R_1 + R_2)$. We emphasize that the periastron distance, R_{min}, is the projected closest approach distance as given by the two-body problem. If the two stars physically collide, the actual closest approach of the center of mass of the two stars will not be exactly equal to this value due to two competing effects. As the dense, low-mass star plunges through the other one, it feels a progressively weaker gravitational pull toward the center of the massive star, which would not occur if the two stars were point masses. On the other hand, friction increases considerably as the impactor penetrates deeper into the target star. We found that, in general, the closest approach is slightly smaller than the one predicted by the two-body problem.

Column (3) of Table 1 gives the fraction of the total mass, $(M_1 + M_2)$, that is lost from the two-star system while column (4) gives the fraction of this ejected mass that originated in Star 1, the more massive one. We computed this mass loss in the same manner as in Paper I. Column (5) gives the number of stars remaining after the encounter. If $N = 0$, the stars have totally broken apart. If $N = 1$, the final system is a coalesced object or a binary. An asterisk in this column means that we were not able to follow the two stars to final coalescence (it would have required too much computer time), but the stars lost enough energy in the initial encounter to become gravitationally bound to each other, so they must eventually either coalesce or form a binary. If $N = 2$ the two stars remain unbound to each other after the encounter. The last two columns, which parameterize the energy dissipation in the collision are discussed below in § 4.2.

4.1. *Descriptions of Typical Encounters*

As in Papers I and II, we can only summarize a small fraction of the tremendous detail shown in these simulations. We shall show the results of a few representative encounters using some of the visual tools we utilize in our analysis.

4.1.1. *Head-on Collision*

Figure 1 gives snapshots of the stars during a head-on collision at parabolic velocity, $V = 0$. The plot shows the velocity vectors of the fluid particles in the collision plane during the encounter. The dimensionless system time, t, given in the plots can be converted to physical units by multiplying it by the factor

$$\tau = 1351[(M_1/M_\odot)(R_\odot/R_1)^{1/2}] \text{ s}, \tag{4.4}$$

which is basically the dynamical time of the system. Figure 2 shows the total specific energies of the two-star system as a function of the system time. The uppermost curve in Figure 2 gives the thermal energy, which increases sharply at the time of physical contact. The next curve gives the large-scale kinetic

© American Astronomical Society • Provided by the NASA Astrophysics Data System

1992ApJ...389..546B

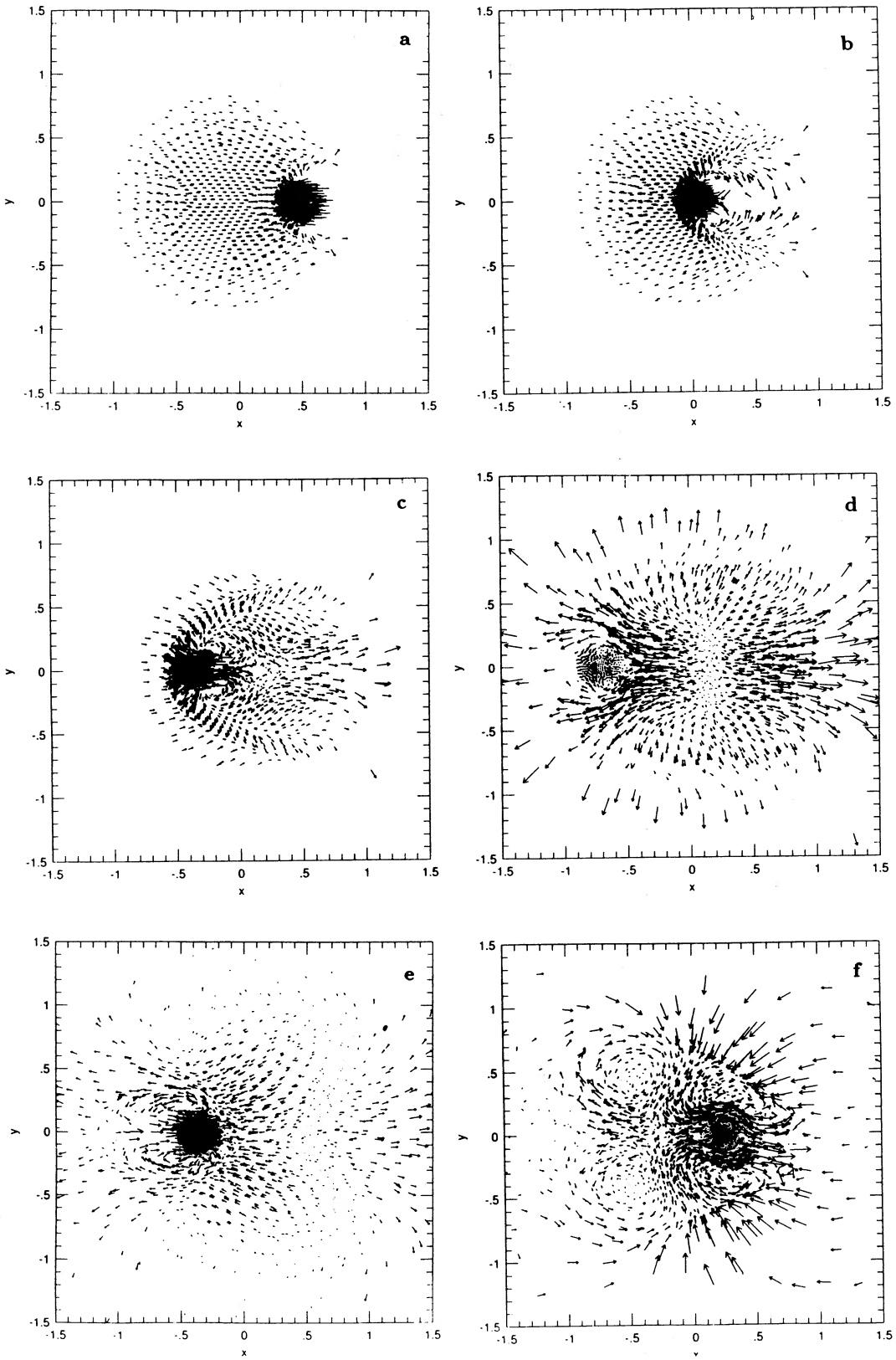

FIG. 1.—Velocity vectors of fluid particles at various times (system time t = 3.54, 3.87, 4.22, 5.19, 6.46, and 8.25) during a parabolic encounter at zero impact parameter. The two colliding lower MS stars differ by a factor of 5 in mass. The lower mass one is the smaller and denser of the two. The unit of system time is given by eq. (4.4).

© American Astronomical Society • Provided by the NASA Astrophysics Data System

1992ApJ...389..546B

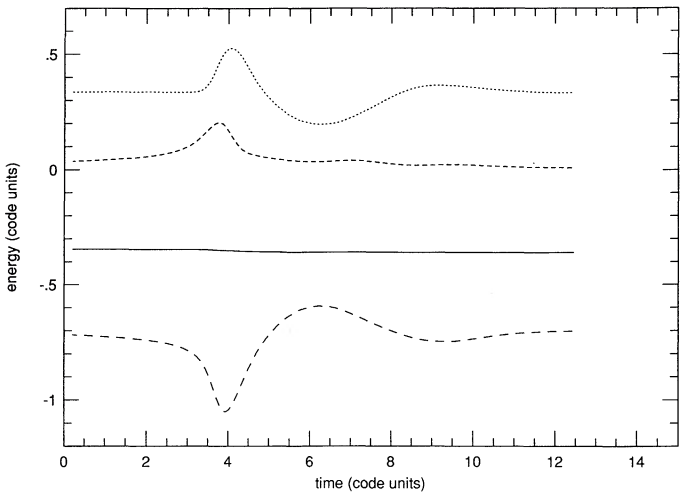

FIG. 2.—Total specific energies as a function of time for the encounter given in Fig. 1. The upper curve gives the thermal energy, which increases at the time of physical contact of the two stars. The next curve gives the large-scale kinetic energy which increases initially as the two stars fall toward each other due to their mutual gravitational attraction. The third curve is the total system energy. The final curve gives the gravitational potential energy.

energy, which initially increases as the two objects fall toward each other by their mutual gravitational attraction and then goes to zero as the two stars fuse into one. The third curve gives the total energy, which remains constant to a fraction of a percent during the encounter. The fourth curve gives the gravitational potential energy.

We notice in Figures 1*b*–1*d*, the formation of a bow shock as the smaller star plows through the more massive one. The low-mass star remains gravitationally self-bound as it passes through the more massive, lower density star. It is compressed by the added pressure it feels as it travels through the more massive star. The maximum pressure, which occurs at the center of the lower mass star, is more than twice as large when this star is passing through the center of the more massive star as it was when the low-mass star first entered it.

The smaller, denser star punches a hole in the more massive, lower density one. The collapse of this hole generates a shock resulting in a high-entropy wake behind the low-mass star. As Figures 1*c*–1*d* show, the shock in turn produces a jet that squirts out of the low-density star at the point where the intruder first entered it. This jet is the primary mass loss mechanism. The remaining mass loss occurs when the intruder breaks out the other side of the low-density star. In Figures 1*e*–1*f* the intruder reenters the more massive star and settles to its center after a few oscillations. In its first passage through the massive star, the low-mass star both increased the entropy of the more massive star enough and decreased its own velocity relative to it enough that it did not produce a significant shock in subsequent passages through it. This allowed a turbulent wake to form, as shown by the vortices that appear behind the reentering intruder. These vortices very efficiently mix the more massive star.

At higher collision velocities, the general behavior is similar except the collisions are more violent and the mass loss is greater. In these higher velocity collisions, the low-density, more massive star becomes strongly elongated in the direction of passage of the low-mass star through it. This elongation significantly increases, i.e., makes less negative, the gravitational potential energy of the star and decreases its gravitational binding energy. At sufficiently high velocities, the hole produced by the lower mass star does not fill in until after this intruder has completely penetrated the lower density, more massive star. In collisions at high velocities and low impact parameters, the low-density star is well mixed after the encounter even if the low-mass star does not coalesce with it. This mixing is due to currents set up in the star as the hole produced by the intruder fills in.

At high enough velocities the two stars are destroyed in low-impact–parameter collisions. The more massive one is destroyed at a lower impact velocity than the less massive one. The more massive star is destroyed by the gravitational perturbations of the low-mass star and by the ram heating it produces in passing through it. The low-mass, denser star is only destroyed by the ram heating it feels in passing through the more massive star. At $V = 2000$ km s^{-1}, the two-star system loses 44% of its mass with over 95% of the loss coming from the more massive star. At $V = 3000$ km s^{-1}, both stars are destroyed. At this velocity, the low-mass star passes through the more massive one largely in one piece, although a wake of debris from it lines the hole it generates in the more massive star. After escaping the more massive star, the low-mass star expands freely to become an unbound cloud. The ram heating it felt in going through the more massive star and its loss of mass is enough to make it gravitationally unbound.

4.1.2. *Grazing Collision*

Figure 3 shows the time variations in the various specific energies for a grazing collision at parabolic speed in which the projected closest approach of the two objects is $R_{\rm min} = 0.757(R_1 + R_2)$. The four specific energies are given in the same order as in Figure 2. Figure 4 shows fluid particles in the star at various critical times during the encounter. The first five frames show the fluid particles that are located within a slice centered on the orbit plane of the two stars. The last frame shows fluid particles in a slice centered on a plane perpendicular to the orbit plane after the low-mass star has settled near the center of the more massive one.

The time variation in the large-scale kinetic energy, which is the second curve from the top in Figure 3, provides a good

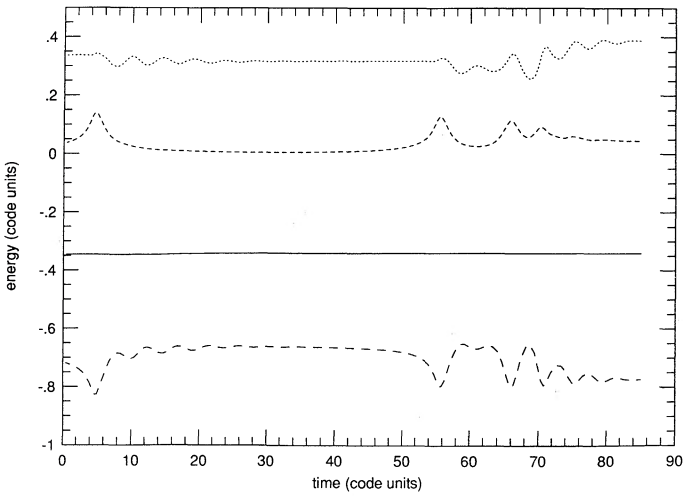

FIG. 3.—The change in the specific energies as a function of time for a parabolic encounter in which the closest approach is $R_{\rm min} = 0.757(R_1 + R_2)$. The order of the specific energies is the same as in Fig. 3.

© American Astronomical Society • Provided by the NASA Astrophysics Data System

1992ApJ...389..546B

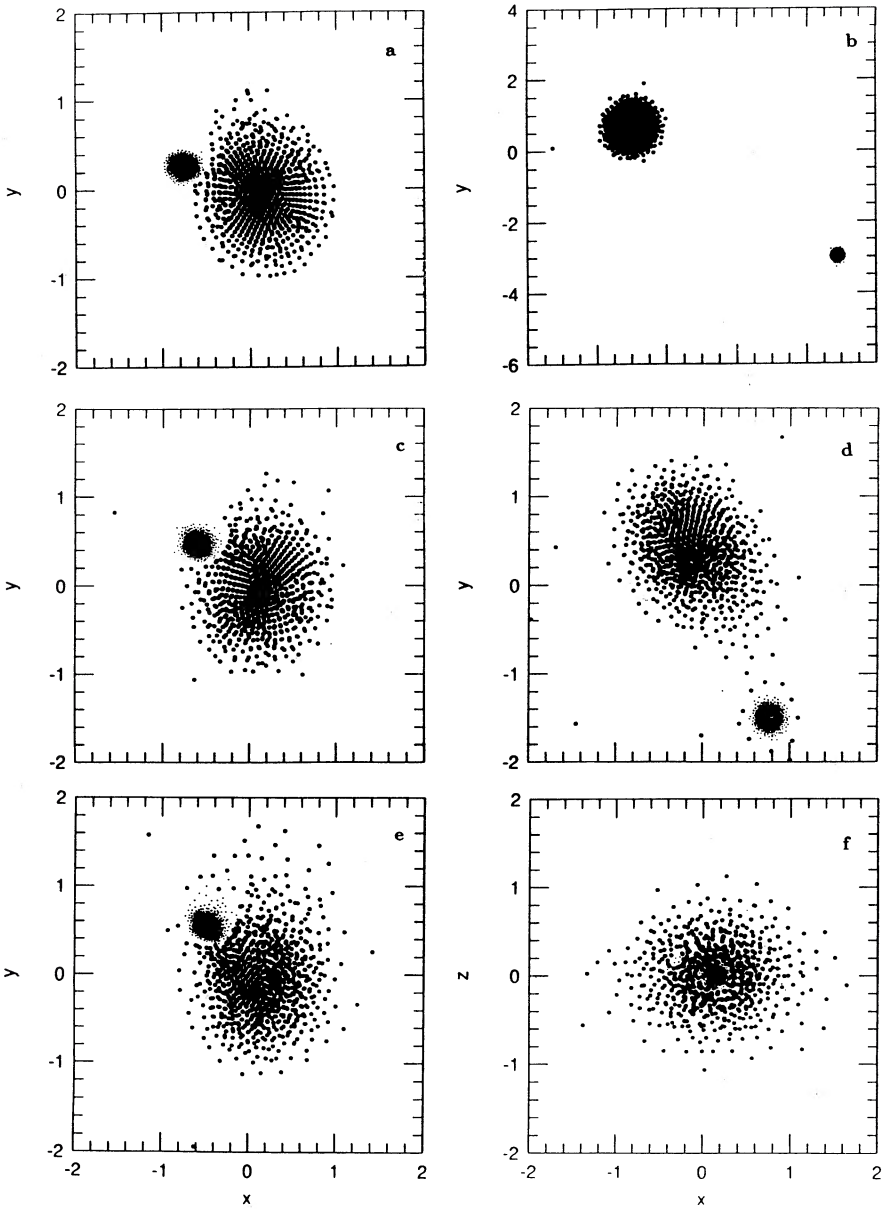

FIG. 4.—The first five frames (*a*–*e*) show the positions of fluid particles in the orbit plane at various times (system times $t = 4.99$, 36.6, 55.9, 62.0, and 66.8) during the encounter given in Fig. 3. The last frame (*f*) shows fluid particles in a plane perpendicular to the orbit plane at a time ($t = 85$) after the low-mass star has settled near the core of the more massive one.

summary of what happened during the encounter. During the first collision, which Figure 4*a* shows, the stars lose enough kinetic energy to become gravitationally bound in a short-period binary orbit. Figure 4*b* shows the two stars near their greatest separation in this orbit. Near time $t = 55$, the stars collide again as Figure 4*c* shows. The energy fed into the more massive star during the first collision causes it to be larger at the second collision, which, consequently, is more violent. After the second collision, the stars are in a more tightly bound orbit, with their greatest separation occurring near the time shown in Figure 4*d*. We see that the low-mass, dense star has accreted an atmosphere of gas that originated in the more massive star. There is also a tongue of gas connecting these two stars during this orbit. The next collision, which Figure 4*e* shows, is even more violent. Figure 3 shows that the two objects go into another bound orbit. Plots of the fluid particles show that the low-mass star orbits inside the more massive one during this stage. Unlike the case for equal-mass stars (Paper I), the merging stars do not form a spiral pattern. The low-mass star rapidly spirals to the center of the more massive star. It is near the center by time $t = 85$.

Figure 3 shows that the postcoalescence kinetic energy approaches 0.05 units rather than zero, as it did for the head-on collision shown in Figure 2. This terminal kinetic energy is the rotational energy of the coalesced star after the encounter. It is $\sim 13\%$ of the final thermal energy, whose time-dependent behavior is given by the top curve in Figure 3. Figure 4*f* shows the fluid particles in a plane perpendicular to the orbit plane after the low-mass star has settled to the center of the more massive one. We see a distinct flattening of the

© American Astronomical Society • Provided by the NASA Astrophysics Data System

1992ApJ...389..546B

star toward the rotational plane, but it has no accretion disk. Accretion disks are produced in grazing collisions between equal-mass MS stars (Paper I) and between white dwarfs (Paper II). The high degree of flattening shown in Figure 4*f* suggests that the star is on the verge of forming a Roche cusp, so it may be near rotational instability. We expect an encounter at a slightly larger $R_{\rm min}$ or one with a slightly more massive secondary star to produce a rotationally unstable, coalesced star.

Jetting in oblique shocks at these impacts produces the mass loss during this encounter. There were three distinct episodes of mass loss corresponding to the three impacts shown in Figure 4. The mass loss at each of the first two impacts was 0.5% while the mass loss in the final impact was 1% for a total system mass loss of 2%.

4.1.3. *Common Characteristics of Collisions*

In both simulations discussed in this section, the denser, low-mass star eventually settles to the center of the less dense, more massive one. All our simulations leading to a single, coalesced star ended with the lower mass star at the center. These mergers thoroughly mix the massive star, so, in particular, the helium accumulated in its core by hydrogen fusion should be mixed throughout it. The amount of nuclear burning that has occurred in the less massive star is nearly negligible if its age is comparable to that of the more massive one. After a Kelvin time the coalesced object should be on the main sequence, but with a helium-rich envelope and a core having the chemical abundance of a zero-age main-sequence (ZAMS) star in the stellar system. This object should be observed in the region of the H-R diagram occupied by the blue stragglers in globular clusters, as predicted by Hills & Day (1976).

This settling of the low-mass star to the center of the more massive one is very different behavior from that found by Cleary & Monaghan (1990) in their simulations of collision between equal-entropy "stars." The more massive of these two "stars" is denser than the less massive one. Their "stars" do not obey the mass-density behavior of MS stars. In collisions between Cleary and Monaghan "stars," the more massive one tidally disrupts the less massive one, so their collisions produce much more mass loss than occurs in collisions between MS stars. Collisions between Cleary & Monaghan "stars" more closely resemble collisions between white dwarfs (Paper II) than between MS stars.

4.2. *Energy Loss*

Column (6) of Table 1 gives V_f, the (effective) velocity at infinity of the two stars after their first collision. We found V_f for those encounters in which the stars either pass near each other and suffer a loss in relative kinetic energy due to tidal dissipation or the small, dense star physically collides with the more massive one but is able to pass through it and comes out its other side. Here V_f^2 is gotten by energy conservation from the separation, s, of the center of mass of the two stars at a time t after the lower mass one has passed by or through the more massive one and from the relative velocity, V_s, of the two stars at this separation. Here

$$V_f^2 = V_s^2 - \frac{2G(M_{1s} + M_{2s})}{s}, \qquad (4.5)$$

where M_{1s} and M_{2s} are the masses of the two stars at time t.

If V_f^2 is positive, the two stars remain unbound and have terminal velocity V_f at infinity. If V_f^2 is negative, the stars have become gravitationally bound, so they must eventually either coalesce into one star or form a binary. To distinguish these bound cases, we have let $V_f = -[\text{abs}\,(V_f^2)]^{1/2}$ for them in Table 1. If no asterisk occurs in column (5) of the table, we followed these bound objects to final coalescence. An asterisk means that we could not follow the long-period binary to either final coalescence or the circularization of the binary orbit.

The last column of Table 1 gives the dissipation velocity, V_d, which parameterizes the kinetic energy lost in the first collision (if there are several) between the two stars. An approach velocity, V_d, at infinity would give the two stars a kinetic energy in their center of mass coordinates equal to that lost in the collision. This velocity is determined from V, the approach velocity at infinity, and from V_f, the postencounter velocity at infinity by the equation

$$V_d^2 = (V^2 - V_f^2) = V^2 - V_s^2 + \frac{2G(M_{1s} + M_{2s})}{s}. \qquad (4.6)$$

Figure 5 shows V_d, the effective loss of velocity due to energy dissipation in the first collision between the stars, plotted as a function of the projected closest approach distance, $R_{\rm min}$. We note that V_d varies smoothly from encounters at $R_{\rm min} \geq (R_1 + R_2)$, where all energy dissipation is tidal to physical collisions at zero impact parameter, where energy dissipation is due both to ram heating and to the production of oscillations in the larger star. There is no change in the slope of V_d versus $R_{\rm min}$ at $R_{\rm min} = (R_1 + R_2)$, which implies that energy dissipation in grazing physical collisions is still largely tidal (gravitationally induced oscillations) rather than due to shock heating. The mass of a star is highly concentrated toward its center, so as the intruder penetrates deeper into the more massive star it can tidally disturb regions closer to its center which contain most of its mass.

V_d is at a maximum if the intruder passes through the center of the more massive star. If the impact velocity, V, of the

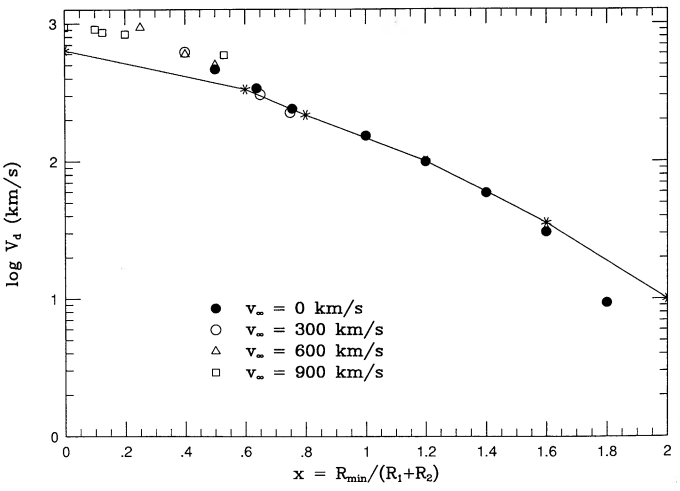

FIG. 5.—The maximum (dissipation) velocity at infinity at which the two stars become gravitationally bound plotted as a function of the projected closest-approach distance for various impact velocities of the intruder at infinity. One star has 0.2 the mass of the MS star. In some encounters the low-mass intruder is another MS star while in others it is a point-mass object (e.g., a white dwarf). The results for the collisions with the point-mass intruder are joined with a line to identify them. The other points correspond to collisions between two MS stars.

© American Astronomical Society • Provided by the NASA Astrophysics Data System

1992ApJ...389..546B

intruder is just enough to allow it to pass through the center of the more massive star and come out its other side, we find that V_d is nearly $1.6V_{esc}$ (which corresponds to 1000 km s^{-1} if M_1 and R_1 have solar values); i.e., for two MS stars to become gravitational bound after a collision at zero impact parameter requires that $V \leq 1.6V_{esc}$. V_d drops to $\sim 0.25V_{esc}$ (150 km s^{-1}) for grazing physical collisions. In the tidal-capture regime we find that V_d drops to $0.02V_{esc}$ (10 km s^{-1}) for $R_{min} = 1.8(R_1 + R_2)$. However, numerical errors result in a small variation of the total energy of the system, ΔE. Assuming that all the error goes into kinetic energy, we can estimate the uncertainty on the velocity to be $\Delta V_d^2 = 2\Delta E/\mu$ where μ is the reduced mass of the system. Typical numbers obtained for ΔE lead to an uncertainty in the dissipation velocity of the order of 10 km s^{-1}. This number although negligible for close encounters is nevertheless too large to allow for an accurate determination of the critical capture radius. We shall later show in this paper that it is likely that V_d drops to 10 km s^{-1} at $(R_1 + R_2) = 2.0$. We note from the figure that the results are not very sensitive to V, the preencounter velocity of the intruder, if $V \leq V_{esc}$. If the intruder penetrates the more massive star and comes out its other side, the energy dissipated is largely independent of the preencounter velocity if $V \leq V_{esc}$.

If all the kinetic energy available in an encounter went to reduce the gravitational self-binding energy of both stars, they would be destroyed if $V/V_{esc} \geq 1.7$, which corresponds to $V \geq 1040$ km s^{-1} for $M_1 = M_\odot$. If the kinetic energy only reduced the binding energy of the more massive star, it would be destroyed if $V/V_{esc} \geq 1.6$ ($V \geq 970$ km s^{-1}). However, the lowest impact velocity at which we observed the stars to be destroyed was at $V/V_{esc} \approx 5$ ($V = 3000$ km s^{-1}). The kinetic energy available in this collision is almost an order of magnitude greater than the minimum needed for disruption of both stars. That the destruction of both stars only occurs at such high velocities show the poor dynamical coupling between them due to their large differences in density and radius.

It is interesting that the maximum velocity V_d at which the two MS stars can still coalesce in a head-on collision is only slightly less than the critical velocity at which the kinetic energy available in the encounter becomes comparable to the gravitational self-binding energy of the more massive star. This may be no coincidence but may be due to much of the energy dissipation even at zero impact parameter being in oscillations set up in the massive star. The energy fed into these oscillations cannot exceed the binding energy of the star, so the energy loss due to tidal dissipation must saturate before the available kinetic energy became comparable to the gravitational binding energy. As we noted earlier, the most massive star becomes very highly elongated in collisions at high velocities near zero impact parameter, so the amplitudes of the oscillations cannot be much larger. For $V \geq V_{esc}$, the massive, low-density star is much larger after the collision, which indicates that the energy fed into it is a large fraction of its initial binding energy.

4.2.1. *Point-Mass Intruder*

To study the relative contribution of ram dissipation and gravitationally induced perturbations (tidal dissipation) in reducing the kinetic energy, we simulated several encounters in which the intruder is a point object with 0.2 the mass of the MS star. Table 2 shows the values of V_d found in these simulations. In the table, R_{min} is given both in units of $(R_1 + R_2) = 1.2532R_1$, the sum of the radii of the two main-sequence stars and in units of R_1. We plot the results in Figure 5.

TABLE 2

MAIN-SEQUENCE VERSUS POINT-MASS ENCOUNTERS: MASSES 5/1

V (km s^{-1})	R_{min} $(R_1 + R_2)$	R_{min} (R_1)	V_d (km s^{-1})
0	0.6	0.75	332.6
0	0.8	1.0	216.8
0	1.2	1.5	100.3
0	1.6	2.0	35.3
0	2.0	2.5	10.0
600	0.0	0.0	637.6
1200	0.0	0.0	467.2
1971.2	0.0	0.0	327.3
2980	0	0.0	237.6

Tables 1 and 2 and Figure 5 show that V_d is nearly the same in encounters with either a pointlike intruder or a MS star of the same mass if $R_{min}/(R_1 + R_2) \geq 0.6$. This indicates both that energy dissipation in these more distant encounters is due to tidal dissipation, gravitationally induced oscillations, and not to ram pressure and that nearly all the dissipation occurs in the larger star. Tidal dissipation is negligible in the denser, lower mass star. We note that for the point-mass intruder V_d drops to 10 km s^{-1} at $R_{min}/(R_1 + R_2) = 2.0$, which is much closer to that expected from extrapolating V_d from its value at smaller values of R_{min} than is the value $R_{min}/(R_1 + R_2) = 1.8$ found for the two MS stars. We believe that the value of 2.0 found with the point-mass intruder is the more likely than 1.8. More evidence to support this point will be given later in this paper.

Unlike the case for grazing collisions, there is a difference in V_d between MS and point-mass intruders for $R_{min} = 0$. The minimum V_d for a MS star going through the center of the more massive star and comining out its other side is ~ 940 km s^{-1} (observed for $V = 900$ km s^{-1}). The corresponding V_d for the point mass (white dwarf) is 640 km s^{-1} (observed for $V = 600$ km s^{-1}), which is the lowest value of V for which we observed the point mass coming out the back side of the MS star. A point mass, e.g., a white dwarf, cannot be captured by a MS star if its impact velocity exceeds 640 km s^{-1}.

Point-mass intruders with $R_{min} = 0$ remained inside the MS star and eventually settled to its center for $V = 0$ and 300 km s^{-1}. For $V \leq V_{esc} \approx 600$ km s^{-1}, the point-mass intruder accretes a substantial amount of mass in its passage through the MS star. The presence of this atmosphere around the point mass greatly increases the dissipation as the intruder moves through the more massive star. For $V \geq 600$ km s^{-1}, the accreted mass becomes negligible and the additional ram dissipation vanishes, so the only remaining dissipation is due to gravitationally induced oscillations.

The difference between the energy dissipation at a given V for the point mass and the finite-size star is purely due to the added dissipation due to ram pressure for the stellar intruder. Figure 6 shows V_d plotted as a function of V for both the MS and point-mass intruders for collisions at zero impact parameter. For the MS star intruder, there is a nearly linear increase in V_d with V due to ram heating. The data in Figure 6 are well fitted by the following relationship

$$V_d = 0.61V + 390 \text{ km s}^{-1} . \quad (4.7)$$

For the point-mass intruder, there is no ram heating for impact velocities $V \geq V_{esc}$, so the dissipation is purely due to

© American Astronomical Society • Provided by the NASA Astrophysics Data System

1992ApJ...389..546B

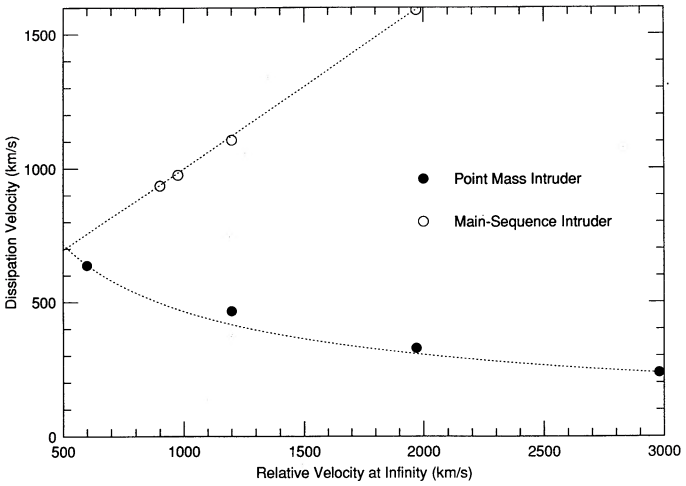

FIG. 6.—Dissipation velocities at zero impact parameter as function of initial impact velocity at infinity. The upper curve is for a collision between two MS stars differing in mass by a factor of 5 and lower curve is between a point-mass object having a mass 0.2 that of the MS star.

gravitationally induced oscillations. This energy dissipation decreases with increasing velocity. This is not surprising. The point mass traverses the same path independently of V. The length of time it spends traversing the path, e.g., the amount of time it spends inside the MS star, is inversely proportional to V if $V \gg V_{esc}$, so the gravitational perturbations and the energy dissipated decrease as V increases. The fitting equation

$$V_d = 640 \text{ km s}^{-1}\left(\frac{V}{600 \text{ km s}^{-1}}\right)^{-0.62} \quad (4.8)$$

gives the relationship between V_d and V for a point mass going through the center of the more massive object. We note that the two curves in Figure 7 converge near $V_d \approx V_{esc} = 600$ km s^{-1} at $V \approx 500$ km s^{-1}.

4.3. *Coalescence*

At low pre-encounter impact velocities, V, the two colliding main-sequence stars eventually coalescence into one if the radii of the two stars overlap at closest approach. As V increases, there is a decrease in the maximum closest approach, R_{fusion}, for which coalescence can occur. R_{fusion} for a given V is the value of R_{min} given in Figure 6 at which $V_d = V$. We show the resulting dependence of R_{min} on V in Figure 7. The figure also shows R_{fusion} for collisions between equal-mass stars as gotten from Figure 5 of Benz & Hills (1987). The values of R_{fusion} from Benz & Hills (1987) are not as accurate as those determined in the current paper. In the earlier paper we used only 500 particles per star and found R_{fusion} by taking the average of the minimum value of R_{min}, where two stars were observed to remain after the encounter and maximum value of R_{min} where fusion into one object was observed.

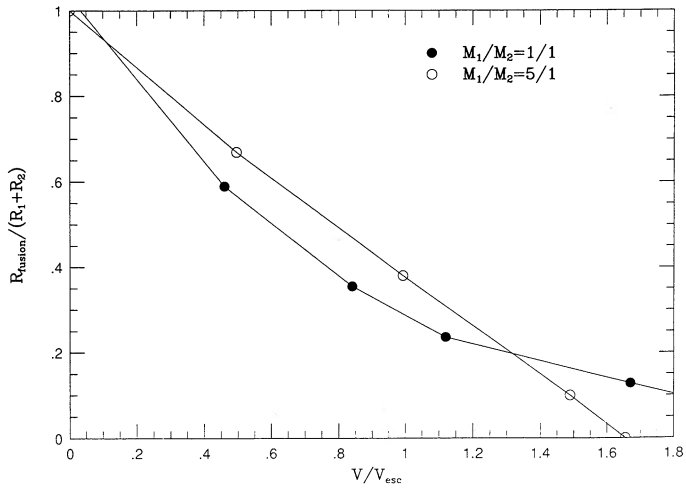

FIG. 7.—The maximum value of the projected closest approach distance at which an encounter would lead to the formation of a single coalesced star. This is plotted as a function of the velocity at infinity given in units of the escape velocity when the two objects are in physical contact.

Our two colliding main-sequence stars do not coalesce even in a zero-impact–parameter collision, if $V/V_{esc} \geq 1.6$. Colgate (1967) first predicted that at a sufficiently large velocity a low-mass MS star can pass through a more massive one without coalescence. An analytic estimate by Sanders (1970) predicted, for the ratio of MS masses used in our simulations, that coalescence does not occur if $V/V_{esc} \geq 3$ or about twice the V found by our full three-dimensional hydrodynamic calculations. Some of this difference may be due to our using a polytrope of index $n = 1.5$ while Sanders used $n = 3$, which is more centrally condensed. The principal deficiency of the analytic model may be its failure to allow for the compression of the low-mass star as it passes through the more massive one. The compression reduces the effective radius and cross section of the low-mass star as it passes through the denser parts of the more massive star.

The data in Figure 7 shows that R_{fusion}, the minimum value of R_{min} needed for coalescence of our two unequal-mass MS stars, is related remarkably well to the impact velocity by the linear equation,

$$\frac{R_{fusion}}{R_1 + R_2} = 0.984 - 0.598\left(\frac{V}{V_{esc}}\right). \quad (4.9)$$

For $V/V_{esc} \leq 1.4$, R_{fusion} for collisions between equal-mass stars is within 20% of the value given by equation (4.9), so this equation may predict R_{fusion} as a function of V to this level of accuracy for all MS stars. The differences in R_{fusion} between the two curves shown in Figure 7 may primarily be due to R_{fusion} being less well determined for the equal-mass stars. That R_{fusion} for equal-mass stars falls off more slowly for $V/V_{esc} \geq 1.4$ is due to jetting in the strong shocks in near head-on collisions. The shocks are much stronger for equal-mass stars because their equal densities do not allow one star to penetrate the other. The jet velocities can be considerably larger than the impact velocity at infinity, so the unjetted material in the stars may lose enough energy to remain gravitationally bound. As Figure 11 of Benz & Hills (1987) shows, the cross section for mass loss in collisions between equal-mass MS stars exceeds that for coalescence if $V/V_{esc} \geq 1.6$. If $V/V_{esc} \geq 1.6$, or $V \geq 1000$ km s^{-1}, collisions between equal-mass MS stars tend to produce a breakdown of the stars into gas rather than their coalescence into more massive objects.

In summary, it appears that in collisions between two lower MS stars, irrespective of their relative masses, coalescence is not important for $V/V_{esc} \geq 1.6$, but the stars tend to be broken apart. In particular, we do not expect the classical diffusion cusps around massive black holes in galactic nuclei to have many stars with mean orbital velocities greater than $2^{-1/2}(1.6V_{esc}) = 1.1V_{esc} = 700$ km s^{-1}. Any stars with much

© American Astronomical Society • Provided by the NASA Astrophysics Data System

1992ApJ...389..546B

higher orbital velocities found orbiting these black holes are likely to be the product of exchange collisions between the black hole and binary stars (Hills 1988).

We have not simulated enough encounters between point-mass objects and MS stars to produce a plot for such encounters corresponding to Figure 7. However, we see in Figure 5 that V_d for these collisions is the same as for collisions between two MS stars if $R_{\rm min} \geq 0.6(R_1 + R_2) = 0.75R_1$. At $R_{\rm min} = 0.75R_1$, $V_d = 350$ km s^{-1}, and then it goes up to its maximum of $V_d = 640$ km s^{-1} at $R_{\rm min} = 0$. These results show that $R_{\rm fusion}$ and the corresponding cross sections for coalescence in collisions between a point-mass intruder and a MS star is the same as between two MS stars if $V \leq 350$ km s^{-1} and then drops to zero for $V = 640$ km s^{-1}. In globular clusters and most galactic nuclei V is low enough that the coalescence cross sections are identical.

The impact parameter, p_c corresponding to the critical closest approach distance, $R_{\rm fusion} = R_{\rm min}$, can be gotten from equation (4.2). The corresponding coalescence cross section, σ, is then

$$\frac{\sigma_c}{\sigma_0} = \frac{\pi p_c^2}{\sigma_0} = \frac{\pi R_{\rm fusion}^2}{\pi(R_1 + R_2)^2}\left(1 + \frac{2a_c}{R_{\rm fusion}}\right) = \frac{R_{\rm fusion}^2}{(R_1 + R_2)^2}\left[1 + \left(\frac{R_1 + R_2}{R_{\rm fusion}}\right)\left(\frac{V_{\rm esc}}{V}\right)^2\right]. \quad (4.10)$$

This equation gives the cross section in units of the geometric cross section, $\sigma_0 = \pi(R_1 + R_2)^2$.

In the limit where the stellar velocity dispersion is much less than the escape velocity from the surface of the colliding stars (which is the case for collisions among MS stars in globular clusters and is a good approximation for the stars in the Galactic center), equation (4.10) reduces to

$$\frac{\sigma_c}{\sigma_0} = \left(\frac{R_{\rm fusion}}{R_1 + R_2}\right)\left(\frac{V_{\rm esc}}{V}\right)^2. \quad (4.11)$$

This limit is appropriate for collisions among MS stars in globular clusters and is a good approximation for collisions among stars in galactic nuclei. We note that the cross section is proportional to $R_{\rm fusion}$ instead of to $R_{\rm fusion}^2$. This is a property of collisions in the limit where gravitational focusing dominates (Hills & Day 1976). In this limit $R_{\rm fusion} = (R_1 + R_2)$, so the coalescence cross section becomes

$$\sigma_c = \pi(R_1 + R_2)^2\left(\frac{V_{\rm esc}}{V}\right)^2. \quad (4.12)$$

The number of collisions per unit volume and time is

$$\frac{dn}{dt} = n_1 n_2 \Gamma, \quad (4.13)$$

where n_1 and n_2 are the space densities of the two species of colliding stars. The rate coefficient for collisions among them in the limit where $V \ll V_{\rm esc}$ and $R_{\rm fusion} = R_1 + R_2$ (Benz & Hills 1987) is given by

$$\Gamma = \langle \sigma_c V \rangle = \pi(R_1 + R_2)^2\left[\left(\frac{3}{\pi}\right)^{1/2}\left(\frac{V_{\rm esc}^2}{\langle V^2 \rangle^{1/2}}\right)\right] \quad (4.14)$$

if their velocity dispersions are independent of their mass. Here $\langle V^2 \rangle$ is the mean-squared velocity dispersion in the system. This equation must be integrated over the volume of the system to find the total collisions per unit time.

4.4. *Tidal Dissipation and Tidal Binaries*

Fabian, Pringle, & Rees (1975) first noted the potential importance of tidally captured binaries in globular clusters. Press & Teukolsky (1977) and more recently Lee & Ostriker (1986) made analytic estimates of the effectiveness of the tidal capture mechanism by assuming linear perturbations.

In a globular cluster, where the impact velocity is typically 10–15 km s^{-1}, Figure 5 shows that tidal captures do not occur if $R_{\rm min}/(R_1 + R_2) \geq 2.0$ for cases where the intruder (either point-mass or MS star) has 0.2 the mass of the target MS star. In those stellar systems where the escape velocity, $V_{\rm esc}$, of the two stars at separation $R_{\rm min}$ is much greater than the velocity dispersion, such as in globular clusters, gravitational focusing is important and the cross section for producing a closest approach with separation $R_{\rm min}$ or less is proportional to $R_{\rm min}$ (eq. [4.11]; Hills & Day 1976; Benz & Hills 1987) instead of to $R_{\rm min}^2$, as in billiard-ball collisions. In globular clusters coalescence of the two stars into one occurs if $R_{\rm min}/(R_1 + R_2) \leq 1$, so tidal capture only occurs for these stars if $R_{\rm min}/(R_1 + R_2)$ lies between 1 and 2. Here the cross section for forming a binary by tidal capture is no larger than that for physical coalescence. As the impact velocity V increases, there is a decrease in the cross section for forming a tidal binary. For $V \geq 0.25V_{\rm esc} = 150$ km s^{-1}, the tidal dissipation is not large enough to allow tidal capture of MS stars. The velocity dispersion is higher than this in the Galactic bulge and in galactic nuclei, so colliding stars in these systems can coalesce or disrupt but not form tidal binaries.

4.4.1. *Point-Mass Intruder*

We found earlier that ram dissipation is not important in grazing collisions and that nearly all tidal dissipation in these collisions occurs in the more massive of the two MS stars. This result suggests that we can replace the less massive MS star by a point mass in studying tidal dissipation in grazing and fly-by encounters. We simulated several encounters in which the intruder is a point object with a mass $M_2 = 0.2$, 0.5, and 1 times the mass, M_1 of the target star. Table 2 gives the results for intruder mass $0.2M_1$ while Table 3 gives them for the more massive intruders. In Table 3, $R_{\rm min}$ is given in units of R_1, the radius of the target main-sequence star.

We find from the data in Tables 2 and 3 that the tidal dissipation velocity, V_d for a given closest approach distance $R_{\rm min}$ is directly proportional to the mass, M_2 of the intruder. This dependence is evident in Figure 8 where we plot $\log_{10}[V_d(M_1/M_2)]$ as a function of $R_{\rm min}$. The plot is nearly a straight line. The spurious point in the figure is the one for $M_2 = 0.2M_1$ and $R_{\rm min}/(R_1 + R_2) = 1.8$, which we noted earlier

TABLE 3

MAIN-SEQUENCE VERSUS POINT-MASS ENCOUNTERS

M_1/M_2	V (km s^{-1})	$R_{\rm min}$ (R_1)	V_d (km s^{-1})
2.....	0.0	1.63	163.0
2.....	0.0	1.96	91.3
2.....	0.0	2.28	44.6
2.....	0.0	2.60	21.2
1.....	0.0	2.0	148.5
1.....	0.0	2.4	68.3
1.....	0.0	2.8	28.6
1.....	0.0	3.2	23.2

© American Astronomical Society • Provided by the NASA Astrophysics Data System

1992ApJ...389..546B

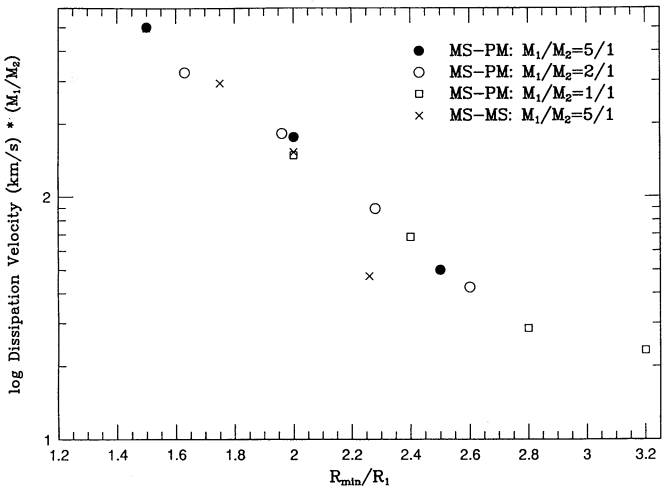

FIG. 8.—The $\log_{10}$ of the dissipation velocities for tidal capture of binaries in nonphysical collisions.

to be too low due to numerical errors. From this figure we find that in a tidal encounter between a MS star of mass M_1 and radius R_1 and a compact object of mass M_2, V_d is related to $R_{\min}$ by the equation

$$V_d = 1520 \text{ km s}^{-1}\left(\frac{M_2}{M_1}\right)\left[\left(\frac{M_1}{M_\odot}\right)\left(\frac{R_\odot}{R_1}\right)\right]^{1/2} \times \exp\left[-2.2\left(\frac{R_{\min}}{R_1} - 1\right)\right]. \quad (4.15)$$

The term in the first square brackets is nearly unity for MS stars. The approximations made in the analytic models suggest that $V_d \propto R_{\min}^{-3}$, which our full three-dimensional simulation shows to be only approximately true. The exponential given in equation (4.15) is clearly a better fit to the data than the analytic power law. In globular clusters, tidal capture occurs if $V_d \leq 10$ km s^{-1}, which requires by equation (4.15) that the closest approach distance be given by

$$\frac{R_{\min}}{R_1} \leq \frac{R_{\text{tidal}}}{R_1} = 3.28 + 0.45 \ln\left(\frac{M_2}{M_1}\right) + 0.22 \ln\left[\left(\frac{M_1}{M_\odot}\right)\left(\frac{R_\odot}{R_1}\right)\right]. \quad (4.16)$$

The right-hand side of this equation is fairly insensitive to the functional parameters since all of them appear inside the two ln terms, so the capture radius is quite sharply defined. For a point mass (e.g., white dwarf) encountering a MS star of the same mass, the tidal capture radius is $R_{\text{tidal}} = 3.28R_1$, so the probability of forming a tidal binary is about twice that the physical coalescence. If two MS stars of equal mass and radius encounter each other, the energy dissipated should be twice that given by an encounter between a point mass and a MS star. In this case, V_d is $2^{1/2}$ times larger than that for a point-mass intruder. Equation (4.15) can be modified to give V_d for this case by replacing 1520 km s^{-1} by 2150 km s^{-1}. To modify equation (4.16) for this case requires that the factor 3.28 be replaced by 3.44; e.g., for encounters between two equal-mass MS stars, the tidal capture radius is $R_{\text{tidal}} = 3.44R_1 = 1.72\ (R_1 + R_2)$ if equal tidal dissipation occurs in each star instead of $R_{\text{tidal}} = 3.28R_1$ if the tidal dissipation occurs in only one object. R_{tidal} increases only 5% if the dissipation doubles. Equation (4.16) should well define the capture radius for lower MS stars. If the two interacting lower MS stars differ even slightly in mass, they differ by a much larger factor in density which results in most of the dissipation occurring in the larger, more massive, lower density star of radius R_1, so equation (4.16) is applicable.

The value of $R_{\text{tidal}} = 3.44R_1 = 1.72(R_1 + R_2)$ for the tidal capture radius of two MS stars of equal mass and radius is smaller than that estimated from analytic work, although the analytic estimates of R_{tidal} have been steadily decreasing with time. Because two equally massive MS stars will coalesce into one object if $R_{\min} \leq (R_1 + R_2)$ (Benz & Hills 1987), the probability that such stars form a binary by tidal capture is only 72% the probability of their coalescence into one star (as the cross section is proportional to $R_{\min}$ in the limit where gravitational focusing dominates, as eq. [4.11] shows). The conditions are a little more favorable for binary capture if the stars are of unequal mass. If they differ by a factor of 5 in mass, we saw earlier that $R_{\text{tidal}} = 2.56R_1 = 2.05(R_1 + R_2)$. Here, the probabilities of coalescence and tidal capture are comparable.

After the binary orbits circularize, conservation of orbital angular momentum results in their semimajor axes being $a_b \approx 2R_{\min} = 2\text{–}4(R_1 + R_2)$ if we ignore the spin angular momenta of the two star. We saw that about one tidal binary forms for every coalesced stars. The stars in a tidal binary have much longer nuclear-burning lifetimes than a coalesced star with their combined mass, so a binary tends to live longer after its formation than a coalesced star of the same mass. The ratio of the number of coalesced stars (a subset of the blue stragglers when the coalesced mass exceeds the mass of the stars at the turnoff point) to the number of tidally captured binaries may be used to place constraints on the maximum space densities of stars reached during the "collapse" phase of "postcollapse" globular clusters and the time that has elapsed since the "collapsed" state.

4.5. *Mass Loss*

Table 1 and Figure 9 show the fraction of mass lost from the two-body system as a function of impact velocity in zero-impact-parameter encounters. For $V/V_{\text{esc}} \geq 1$, the mass loss increases nearly exponentially from $\sim$2% to total breakup of both stars at $V \approx 5V_{\text{esc}} = 3000$ km s^{-1}.

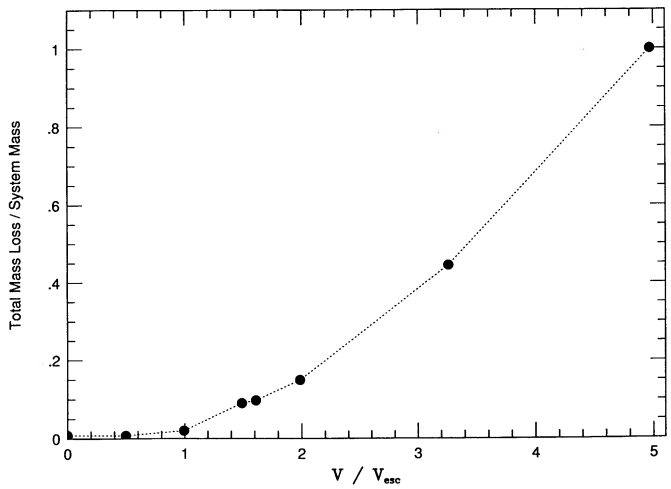

FIG. 9.—The fraction of the mass lost from the system as function of impact velocity at zero impact parameter. The velocity is given in units of the escape velocity of the objects when they are in physical contact.

© American Astronomical Society • Provided by the NASA Astrophysics Data System

1992ApJ...389..546B

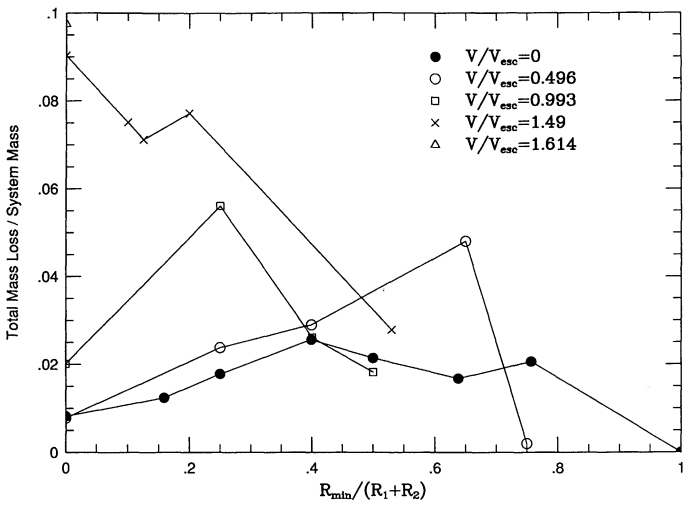

FIG. 10.—The fraction of the mass lost from the system at a function of the projected closest approach distance for various values of the impact velocity. The projected closest approach distance is given in units of the radii of the two stars while the velocities are given in units of the escape velocity at physical contact of the two stars.

Figure 10 shows the fraction of mass lost from the two-star system plotted as a function of $R_{\min}/(R_1 + R_2)$ for the various values of the impact velocity V. For equal-mass stars (Benz & Hills 1987), the mass loss for $V \ll V_{\rm esc}$ is at a maximum for grazing collisions due to the gravitational torquing of each star by the other and to the large amount of angular momentum in the coalesced objects. This mechanism is not important in collisions between our unequal-mass stars. For collisions between these stars, jetting in oblique shocks is responsible for the mass loss. These shocks tend to be very weak in grazing collisions.

We may use the procedure given in Paper I to compute the mass-loss cross sections from the data given in Figure 10. The results are given in Table 4. The mass-loss cross section $\sigma_{\rm ML}$ is given in units of the geometric cross section, $\sigma_0 = \pi(R_1 + R_2)^2$, in column (2) and in terms of the coalescence cross section, $\sigma_{\rm fusion}$, in column (4). The mass-loss cross section is defined such that the rate of mass loss per unit volume due to collisions between two species of MS stars of mass M_1 and M_2 with

TABLE 4

MASS-LOSS AND COALESCENCE CROSS SECTIONS

V (km s^{-1})	$\sigma_{\rm ML}$ (σ_0)	$\sigma_{\rm fusion}$ (σ_0)	$\sigma_{\rm ML}$ ($\sigma_{\rm fusion}$)
→0	$0.016(V_{\rm esc}/V)^2$	$1.0(V_{\rm esc}/V)^2$	0.0161
300	0.0625	3.165	0.0198
600	0.0331	0.529	0.0626
900	0.0309	0.055	0.562

space densities n_1 and n_2 is given by the equation

$$\frac{dM}{dt} = (M_1 + M_2) n_1 n_2 \langle \sigma_{\rm ML} V \rangle \, . \qquad (4.17)$$

4.5. *Kick Velocity of Coalesced Object*

The asymmetric jetting of ejected material in the collision of the two stars acts as a rocket that propels the coalesced star away from the center of mass of the original two-body system. This kick velocity is primarily of concern in globular clusters, which have low escape velocities. We find for the case where the impact velocity $V = 0$ at infinity that the kick velocity is 4.4 km s^{-1} and 4.7 km s^{-1} for $R_{\min}/(R_1 + R_2) = 0.25$ and 0.50, respectively.

A kick velocity of $V_k = 4.5$ km s^{-1}, is not large enough to eject the coalesced star from the core of a globular cluster, but it significantly reduces the dynamical "cooling" that otherwise occurs when two stars coalesce into one. The relative velocity at infinity in a globular cluster is typically $V = 10$–15 km s^{-1}. The kinetic energy associated with this velocity, $E_c = 0.5\,[(M_1 M_2)/(M_1 + M_2)]V^2$, would be lost to the globular cluster in the coalescence of these two stars. The kick velocity introduces a kinetic energy to the cluster of $E_k = 0.5\,(M_1 + M_2)V_k^2$. For $M_2 = 0.2M_1$, $V = 12$ km s^{-1} and $V_k = 4.5$ km s^{-1}, $E_k = E_c$, so the coalescence of the stars produces no net dynamical cooling in the cluster. Coalescence does not seem capable of significantly accelerating the collapse of the core of a stellar cluster.

This research was supported in part by NASA grant NGR 22-007-272 and DOE. One of us (W. B.) also acknowledges partial support from the Swiss National Science Foundation.

REFERENCES

Benz, W. 1990, in Numerical Modeling of Nonlinear Stellar Pulsations, ed. J. R. Buchler (Dordrecht: Kluwer Academic)
Benz, W., Bowers, R. L., Cameron, A. G. W., & Press, W. H. 1990, ApJ, 348, 647
Benz, W., & Hills, J. G. 1987, ApJ, 323, 628 (Paper I)
Benz, W., Hills, J. G., & Thielemann, F.-K. 1989, ApJ, 342, 986 (Paper II)
Cleary, P. W., & Monaghan, J. J. 1990, ApJ, 349, 150
Colgate, S. A. 1967, ApJ, 150, 163
Davies, M. B., Benz, W., & Hills, J. G. 1991, ApJ, 381, 449
Fabian, A. C., Pringle, J. E., & Rees, M. 1975, MNRAS, 172, 15p
Hernquist, L., & Katz, J. 1989, ApJS, 70, 419
Hills, J. G. 1978, MNRAS, 182, 517
———. 1988, Nature, 331, 687
Hills, J. G., & Day, C. A. 1976, Ap. Lett., 17, 87
Lee, H. M., & Ostriker, J. P. 1986, ApJ, 310, 176
Monaghan, J. J. 1985, Comput. Phys. Rept., 3, 71
Monaghan, J. J., & Lattanzio, J. C. 1985, A&A, 149, 135
Press, W. H., & Teukolsky, S. A. 1977, ApJ, 213, 183
Sanders, R. H. 1970, ApJ, 162, 791

© American Astronomical Society • Provided by the NASA Astrophysics Data System